EPJ manuscript No.
(will be inserted by the editor)

Phase-Imaging Ion-Cyclotron-Resonance technique at the JYFLTRAP double Penning trap mass spectrometer

D.A. Nesterenko [a], T. Eronen, A. Kankainen, L. Canete, A. Jokinen, I.D. Moore, H. Penttilä, S. Rinta-Antila, A. de Roubin, and M. Vilen

University of Jyväskylä, P.O. Box 35, FI-40014 University of Jyväskylä, Finland

Received: date / Revised version: date

Abstract. The Phase-Imaging Ion-Cyclotron-Resonance (PI-ICR) technique has been commissioned at the JYFLTRAP double Penning trap mass spectrometer. This technique is based on projecting the ion motion in the Penning trap onto a position-sensitive multichannel-plate ion detector. Mass measurements of stable $^{85}Rb^+$ and $^{87}Rb^+$ ions with well-known mass values show that relative uncertainties $\Delta m/m \leq 7 \cdot 10^{-10}$ are possible to reach with the PI-ICR technique at JYFLTRAP. The significant improvement both in resolving power and in precision compared to the conventional Time-of-Flight Ion Cyclotron Resonance technique will enable measurements of close-lying isomeric states and of more exotic isotopes as well as ultra-high precision measurements required, e.g., for neutrino physics. In addition, a new phase-dependent cleaning method based on the differences in the accumulated cyclotron motion phases has been demonstrated with short-lived $^{127}In^+$ and $^{127m}In^+$ ions.

PACS. 21.10.Dr – 07.75.+h – 37.10.Ty

1 Introduction

Accurate mass values of atoms are essential for various fields of physics [1,2]. For example, nuclear binding energies needed for understanding the evolution of nuclear structure far from stability and for nuclear astrophysics can be derived from atomic masses. Typically these nuclei are short-lived with low production rates requiring fast and accurate methods to determine their masses. In fundamental physics studies, e.g. to test the Standard Model of Particle Physics or for neutrino studies, ~~rather high-precision ($\leq 10^{-9}$) for~~ where accurate mass differences (Q-values) are necessary, rather high-precision ($\leq 10^{-9}$) for masses is required [3,4].

Penning-trap mass spectrometry is the most accurate and widely used method for high-precision atomic mass measurements at the moment. Conventionally, Penning trap mass spectrometry of short-lived ions has employed the Time-of-Flight Ion Cyclotron Resonance (ToF-ICR) [5,6] technique to determine ion cyclotron frequency in a strong uniform magnetic field B:

$$\nu_c = \frac{1}{2\pi}\frac{q}{m}B, \qquad (1)$$

where q and m are the charge and the mass of the ion, respectively. Additional three-fold gain in precision can be achieved using Ramsey method of temporally separated oscillatory fields (Ramsey ToF-ICR) [7,8,9]. The ToF-ICR method can provide a relative mass accuracy of better than 10^{-8} [3,10,11] when 1−5 ions/s is detected. For ions with lower production rates (< 1 ion/s) or with short half-lives (< 100 ms) precision in the order of 10^{-7} has been typically reached ~~[12]~~[13].

Recently, a novel approach to measure the ion cyclotron frequency (see Eq. (1)) has been developed at SHIPTRAP double Penning trap mass spectrometer [14, 15] at GSI. This Phase-Imaging Ion-Cyclotron-Resonance (PI-ICR) technique is based on projecting the ion motion in a Penning trap onto a position-sensitive ion detector. It has been shown to offer a 40-fold increase in the resolving power and a fivefold gain for the precision of the cyclotron-frequency determination compared to the Ramsey ToF-ICR technique. The PI-ICR technique has been applied for high-precision determination of mass differences of stable and long-lived nuclides at SHIPTRAP [16, 17,18]. In this article, we report on the implementation of the PI-ICR technique at the JYFLTRAP double Penning trap mass spectrometer [19] at the IGISOL facility in the Accelerator Laboratory of the University of Jyväskylä. A measurement of the mass difference of stable ^{85}Rb and ^{87}Rb isotopes whose mass values are very well known with precisions of 5 and 6 eV/c^2 [20], respectively, was demonstrated.

A critical prerequisite for high-precision Penning trap mass measurements is that the studied ion sample consists only of ions of interest. Other ions (contaminants) can cause frequency shifts [21] due to their different mass (see Eq. (1)), and in the worst case make a mass measure-

[a] e-mail: dmitrii.nesterenko@jyu.fi

ment impossible. A high resolving power is essential not only for mass measurements but also for state-selective decay spectroscopy (for details and examples, see the recent review [2]).

Penning trap setups for short-lived ions typically rely on sideband cooling technique to remove contaminants [22]. Mass resolving power $m/\Delta m$ of about 10^5 can be reached with this technique, which is often sufficient for separating isobars. With a buffer-gas free cleaning SIMCO (SImultaneous Magnetron and resonant COnversion) method [23] a resolving power up to $7 \cdot 10^5$ can be reached. Also multi-reflection time-of-flight (MR-ToF) separators are available with mass resolving power of few$\times 10^5$ [24]. Many nuclei have long-living isomeric states that require even higher mass resolving power than these techniques are able to provide. In order to separate states with excitation energies of a few tens of keV, a mass resolving power $m/\Delta m$ exceeding 10^7 is needed. This is challenging with the present cleaning methods.

The resolving power in the ToF-ICR technique is proportional to the excitation time in the trap and is ultimately limited by the half-life of the studied nuclei. For singly-charged ions of medium-heavy ($A \approx 100$) radionuclides with half-lives of about 1 s or longer, a resolving power of about 10^6 ($\nu_c \approx 1$ MHz in a 7-T magnetic field) is reached meaning that only states differing by several hundreds of keV can be separated. A method using an octupolar conversion of ion motion [25,26] can increase the resolving power by an order of magnitude compared to the ToF-ICR method with a conventional quadrupolar conversion. However, it does not improve the precision. Highly-charged ions could increase both the precision and the resolving power but that would require an additional step of ion-charge breeding, which imposes strict restrictions on the vacuum in the trap and a number of other challenges [27].

Typically, states separated by ≈ 100 keV or more can be resolved with a Ramsey cleaning technique [28]. It enables contaminant-free mass measurements by separating and removing unwanted ions using an additional cleaning step lasting ≈ 100 ms before the ToF-ICR measurement. Unfortunately, the number of ions the Ramsey cleaning technique can handle has been found to be quite small. If there are a lot of contaminant ions present, the number of ions entering the trap has to be limited, and thus the overall transmission is reduced.

In this article, we present a new fast cleaning method (see Sect. 2.3) which can offer a much higher resolving power compared to previous techniques. This phase-dependent cleaning technique is demonstrated by using the separation of the ground and isomeric states of ^{127}In as an example in Sect. 3.4.

2 Phase-Imaging Ion-Cyclotron-Resonance technique

2.1 Ion motion in a Penning trap

An ion is confined in a Penning trap by the superposition of a strong homogeneous magnetic field $\boldsymbol{B} = B_z \boldsymbol{e}_z$ and a quadrupolar electrostatic potential. In cylindrical coordinates (z, ρ), the potential has the form:

$$V(z,\rho) = \frac{U_0}{2d^2}(z^2 - \rho^2/2), \tag{2}$$

where z and $\rho = \sqrt{x^2+y^2}$ are the axial and radial distance from the trap center, respectively, U_0 is the trap potential (the potential difference between the ring and the endcap electrodes [19]) and ~~$d = \sqrt{2z_0^2 + r_0^2}$~~ d is the characteristic dimension of the trap defined by the trap geometry~~[19]~~. For ideal hyperbolic traps $d = \sqrt{2z_0^2 + r_0^2}/2$, where $2z_0$ is the distance between endcap electrodes and r_0 is the inner radius of the ring electrode [29]. In reality, z_0 and r_0 differ (especially for a cylindrical trap geometry [30]) from the ideal case.

The trajectory of an ion in the trap is a superposition of three independent harmonic eigenmotions: axial motion at frequency ν_z along the magnetic field lines and two radial motions perpendicular to the magnetic field lines. Of the radial motions, the magnetron motion with a frequency ν_- is almost mass-independent whereas the cyclotron motion's frequency, although reduced to the modified cyclotron frequency ν_+, remains mass-dependent. In an ideal Penning trap, the sum of the two radial motion frequencies is the ion cyclotron frequency ν_c:

$$\nu_c = \nu_+ + \nu_-. \tag{3}$$

Even with small misalignments of the magnetic and electric fields and ellipticity of the trapping potential, Eq. (3) is precise enough for mass measurements with current Penning trap techniques for short-lived ions [31]. The hierarchy of the frequencies is $\nu_c \approx \nu_+ \gg \nu_z \gg \nu_-$ [29]. The modified cyclotron frequency, the magnetron frequency and the axial frequency for $^{133}Cs^+$ ions at the JYFLTRAP (see Sec. 3.1) are $\nu_+ \approx 807$ kHz, $\nu_- \approx 1.7$ kHz and $\nu_z \approx 52$ kHz.

The operation of a Penning trap is based on the manipulation of the ion eigenmotions through the application of radiofrequency (RF) fields in different configurations. A dipolar excitation at an eigenfrequency of the ion (ν_+, ν_-, ν_z) can be used to excite the corresponding ion motion. An RF quadrupolar field at the cyclotron frequency ν_c can convert one radial motion to the other [6]. The ring electrodes of JYFLTRAP are eight-fold segmented [19], and thus, dipolar, quadrupolar and even octupolar RF fields can be applied.

2.2 Principle of the Phase-Imaging Ion-Cyclotron-Resonance technique

A detailed description of the PI-ICR technique is given in Ref. [15]. There are two ways to determine ν_c of Eq.

(3); either by measuring both magnetron and modified cyclotron frequencies independently (see Sect. 2.2.1) or quasi-simultaneously (see Sect. 2.2.2).

In the following, we denote the values related to the magnetron and cyclotron motion by the indexes "-" and "+", respectively. With the word "radial", we will mean either a "magnetron motion" or a "cyclotron motion"; in this case the indexes are omitted.

2.2.1 Radial motion frequency measurement

The principle of the measurement is illustrated in Fig. 1. After buffer-gas cooling [22] in the preparation trap, the ions are injected into the center of the measurement trap (see Sec. 3.1) and have a spatial distribution with FWHM= $2\Delta r$ (position 1 in Fig. 1). Then the ions are excited with a dipolar pulse at the radial frequency ν, and they reach a certain radius of motion (position 2 in Fig. 1). After free revolution for a duration t the ion motion accumulates a phase $\varphi + 2\pi n = 2\pi\nu t$, where n is a full number of revolutions (position 3 in Fig. 1). Here the positions 1, 2 and 3 are the trap center, the reference phase and the final phase, respectively.

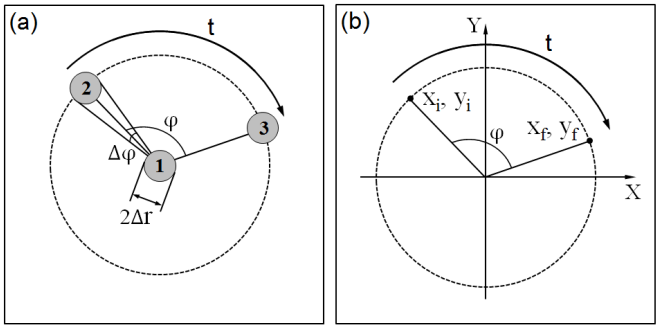

Fig. 1. Radial motion frequency measurement in a Penning trap. (a) The position 1 indicates the trap center where the ions have been injected. After excitation to a certain radius, the ions are at position 2 (reference phase). At position 3 (final phase) ions have rotated freely for time t ending up to an angle φ relative to the reference phase. (b) The coordinates of the reference phase (x_i, y_i), the final phase (x_f, y_f) and the phase angle φ. The magnetic field is perpendicular to the plane of the figures.

In reality, ions gain initial magnetron motion due to misalignments between the magnetic field and the trap axis and also some axial motion after the injection into the measurement trap. Fortunately both of these are coherent and thus amplitudes of these motions can be reduced via dipolar RF pulses with the matched amplitudes and phases at the corresponding motion frequencies.

For simplicity, the electric potential center of the traps is set as the origin, $(0, 0)$ in the following. The phase angle φ is deduced from the coordinates of the reference phase (x_i, y_i) and the final phase (x_f, y_f) . The radial frequency ν and its uncertainty $\delta\nu$ can be calculated as

$$\nu = \frac{\varphi + 2\pi n}{2\pi t},\ \delta\nu = \frac{\delta\varphi}{2\pi t} = \frac{\delta s}{2\pi t\sqrt{1-s^2}}, \qquad (4)$$

where $\varphi = \arccos(s)$ for $0 \le \varphi \le \pi$ and $\varphi = 2\pi - \arccos(s)$ for $\pi \le \varphi \le 2\pi$, and $s \equiv \cos(\varphi) = (x_i x_f + y_i y_f)\ /\ (\sqrt{x_i^2 + y_i^2}\sqrt{x_f^2 + y_f^2})$. The direction of the radial motion and, correspondingly, the correct value for the angle can be determined from the projection image. A quick measurement of the radial frequency with a modest precision (with a shorter phase-accumulation time than for the main measurement) allows to get the integer number of revolutions n in Eq. (4). It is enough to perform such measurements once per several days, since the typical daily fluctuations of the magnetron and modified cyclotron frequencies do not exceed 100 mHz at JYFLTRAP.

The ion radial motion is projected onto a position-sensitive ion detector (microchannel plate detector with a delay line anode) placed on the axis of the trap outside the magnet (see Fig. 3) to determine the accumulated phase and deduce the radial frequency. The ideal projection magnifies the image on the detector relative to the ion motion in the trap and preserves the angle φ.

In order to determine the angle φ and the corresponding radial frequency, coordinates for the trap center, the reference phase and the final phase on the detector have to be measured.

After the injection of the ions into the measurement trap and reducing of the residual magnetron and axial motions, the ions are extracted from the trap and projected onto the detector to determine the coordinates of the trap center. The stability of the trap center position depends on the stability of electric potentials both on the trap electrodes and those in the drift section after the magnet. Usually, it is enough to measure the center once a day. To find the position of the reference phase, the ions are extracted from the trap right after applying the dipolar RF pulse at radial frequency ν. Extraction of the ions after a fixed time t later than for the reference phase allows the projection of the final phase to be measured (see Fig. 1).

The projection of the cyclotron motion phase requires an additional step. Since the width of the time-of-flight distribution of ions between the trap and the detector is comparable with the period of the cyclotron motion (both about $1\,\mu$s for $^{133}Cs^+$, as example), a direct projection would lead to a smearing of the ion spot on the detector (see Fig. 5b). Therefore, before extracting the ions, the fast cyclotron motion has to be converted to the slow magnetron motion by applying a short radial quadrupolar pulse at the cyclotron frequency ν_c of the ions. The conversion preserves the modulus of the angle between the reference and the final phase of the corresponding motions and flips the sign of the angle [15,32]. Thus, the ion cyclotron motion and the movement of the image on the detector have opposite angular directions (in case of JYFLTRAP the image of the magnetron motion rotates clockwise and the image of the cyclotron motion rotates

counterclockwise on the detector looking downstream in the beamline).

2.2.2 Cyclotron frequency measurement

The cyclotron frequency ν_c can be determined directly by applying two excitation patterns alternately (Fig. 2). The patterns are identical except for the starting time of the quadrupole excitation. First, like in radial motion frequency measurement, the cooled and centered ions are transferred from the first trap to the center of the measurement trap (step 1), where the coherent component of their magnetron and axial motions are reduced via dipolar RF pulses at the corresponding motion frequencies (steps 2a and 2b). Then, the cyclotron motion of the ions is excited via a dipolar RF pulse at the frequency ν_+ and the ions acquire a certain radius of motion (step 3). In step 4 of pattern 1 a quadrupolar RF pulse at the cyclotron frequency ν_c is applied immediately after the ν_+-pulse to convert the cyclotron motion to the magnetron motion. After the conversion, ions rotate freely and the magnetron motion accumulates total magnetron phase

$$\varphi_-^{\text{tot}} = \varphi_- + 2\pi n_- = 2\pi\nu_- t, \tag{5}$$

where $\varphi_- \in [0, 2\pi)$ is the final phase and n_- the integer number of revolutions after time t. Subsequently, the ions are ejected from the trap and their position is projected onto the position-sensitive ion detector (step 5). Pattern 2 differs from pattern 1 only in step 4. The quadrupolar conversion pulse at the cyclotron frequency ν_c in pattern 2 is applied after the time t from the ν_+-pulse, allowing ion motion to accumulate total cyclotron motion phase

$$\varphi_+^{\text{tot}} = \varphi_+ + 2\pi n_+ = 2\pi\nu_+ t, \tag{6}$$

similarly as for magnetron motion phase. After conversion, the ions are projected onto the detector giving the image of the cyclotron motion phase.

As noted earlier, the conversion preserves the modulus of the angle between the reference and the final phase and flips the sign of the angle [15,32]. Thus, the polar angles of the spot position on the detector are $\alpha_- = \alpha_0 - \varphi_-$ and $\alpha_+ = \alpha_0 + \varphi_+$ for the accumulated magnetron and cyclotron motion phases, respectively, where α_0 is the polar angle of the initial phase. Hence, the angle between the positions of two phase images is $\alpha_c = \alpha_+ - \alpha_-$ and the cyclotron frequency ν_c is

$$\nu_c = \frac{\alpha_c + 2\pi(n_+ + n_-)}{2\pi t}. \tag{7}$$

In order to eliminate the error of the conversion of radial motions, the phase accumulation time must be a multiple of a half the period of the cyclotron motion, *i.e.*, $2\pi\nu_c t = \pi n$ [15,32]. The durations of the excitation pulses can be chosen as short as the period of the corresponding RF excitation frequency. The main reason for short duration is to save measurement time but short pulse also ensures equally strong excitation in large frequency band. In practice they are limited by the available maximum amplitudes of the function generators (10 V in case of JYFLTRAP). A typical RF pulse duration at JYFLTRAP is 1 ms, which covers ~~around 1 kHz~~ a 1-kHz band around the applied excitation frequency.

2.3 Phase-dependent cleaning method

The resolving power of the ToF-ICR method is defined by Fourier transformation of the excitation time profile and limited by the excitation time t_{exc} or the observation time of the cyclotron motion [33]. The line width of the Fourier-transformation in the frequency domain $\Delta\nu_c$(FWHM) is inversely proportional to the excitation time t_{exc}. The resolving power obtained with the ToF-ICR method and a single quadrupolar excitation (conversion) pulse [34,35] is

$$R = \frac{m}{\Delta m} = \frac{\nu_c}{\Delta\nu_c} \approx \nu_c t_{exc}. \tag{8}$$

Since the magnetron frequency depends only very weakly on the mass of the ion, the resolving power of the PI-ICR method is defined by the ability to resolve the phase difference of cyclotron motions between two ion species after accumulating for a time t (see Fig. 1):

$$R = \frac{\nu_+}{\Delta\nu_+} = \frac{2\pi t}{\Delta\varphi}\nu_+ \approx \frac{\pi t r_+}{\Delta r_+}\nu_+. \tag{9}$$

For a typical in-trap radius spread $\Delta r_+ = 80$ μm and excitation radius $r_+ = 1$ mm, the PI-ICR method provides around 40 times better resolving power than the ToF-ICR method.

The following phase-dependent cleaning method is suitable for preparing isomerically pure beams for post-trap decay spectroscopy. After the mass-selective buffer-gas cooling [22] procedure in the preparation trap that provides a resolution of a few tens of Hz for $\Delta\nu_c$ (corresponds to $\sim 10^5$ in mass resolving power for singly charged A=100 ions in 7 T field), ions are injected to the center of the measurement trap. A short dipolar rf pulse (about 1 ms) at the modified cyclotron frequency ν_+ will excite any remaining ions to a certain radius r_+ since the FWHM of the excitation with 1 ms duration is about 1 kHz. The ion motion accumulates the phase difference $\Delta\varphi$ for a time t, which is chosen to be long enough to resolve the ions of interest and the contaminants. Then, a short quadrupolar RF pulse at the cyclotron frequency ν_c is applied just before the extraction of ions to convert the cyclotron motion to magnetron motion. Ions leave the trap and are projected onto the position-sensitive ion detector. The image of the ion motion projection allows the ions of interest and contaminant ions to be distinguished. By positioning movable and adjustable slits ~~before~~ in front of the detector according to the position of the ions of interest on the detector the contaminants can be removed. Then, after removing the detector from the ion's way, a cleaned beam of the ions of interest can be transported to the experiment setups further downstream.

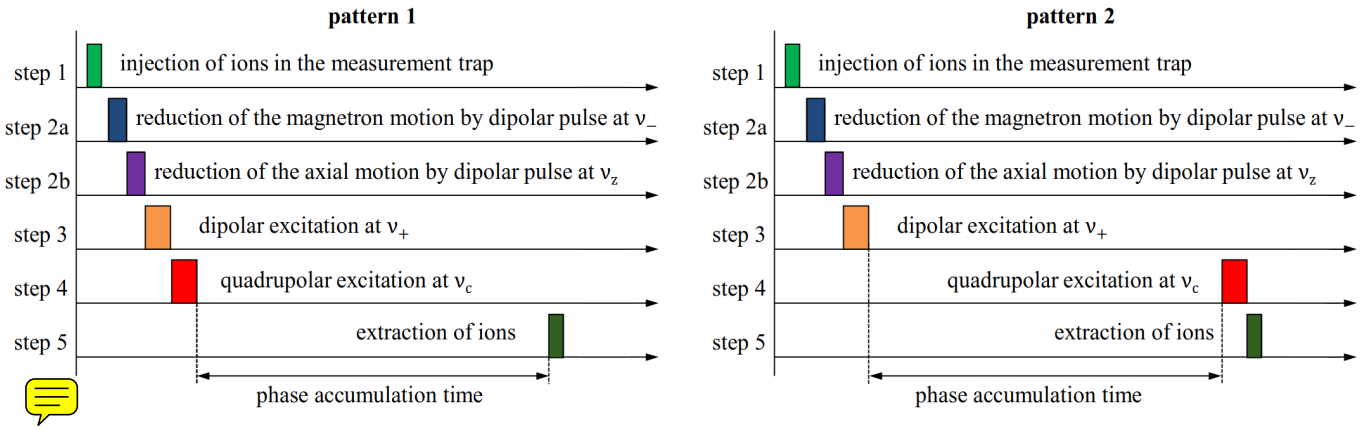

Fig. 2. Measurement sequence where the cyclotron frequency ν_c is determined with the PI-ICR technique. The magnetron and cyclotron phases are accumulated in the patterns 1 and 2, respectively.

If the accumulated phase difference $\Delta\varphi$ between the ions of interest and contaminants is about π, the cleaning method can be performed without the slits ~~before~~ in front of the detector. One more dipolar RF excitation step at the magnetron frequency ν_- before the extraction of ions is needed. The phase and the amplitude need to be matched so that the ions of interest will move to the trap center. Since the contamination ions are on the opposite phase, they will move even further out and finally acquire magnetron radius $2r_+$. If the radius of the contaminants is large enough, they will be lost during the transportation from the trap, while the centered ions of interest will survive.

A similar idea for the cleaning procedure, based on the mass-selective ion centering, was described in [36]. The authors in [36] suggested to use a pulsed static dipolar excitation to center the ions of interest, in contrast to the magnetron excitation pulse presented in this work.

3 PI-ICR technique at JYFLTRAP

3.1 The JYFLTRAP setup

The JYFLTRAP double Penning-trap setup is extensively used for high-resolution beam purification and precise mass measurements of stable and radioactive ions [19]. The JYFLTRAP setup receives on-line beams from the Ion Guide Isotope Separator On-Line (IGISOL) facility [37]. The radioactive ions, produced either by fission or fusion reactions, are stopped in helium gas, extracted by using electric fields and a helium gas jet via a sextupole ion guide [38] to high-vacuum, where the ions are accelerated to $30z$ keV energy (z is the charge state of the ions). Behind a 55° dipole magnet ($M/\Delta M \approx 500$), ions with the selected mass-to-charge ratio A/q are injected into a gas-filled radio-frequency quadrupole (RFQ) [39], where they are cooled and bunched. For offline measurements a surface-ionization ion source or laser-ablation ion source can be mounted in front of the RFQ cooler.

The ion bunches from the RFQ are transferred to the cylindrical Penning traps placed inside a 7-T superconducting magnet ~~.~~ (Fig. 3). In the first, gas-filled ($10^{-4}\ldots10^{-5}$ ~~-~~mbar of helium), preparation trap the ions are cooled, centered and purified via a mass-selective buffer gas cooling technique [22]. The ions are transferred through a diaphragm 1.5 ~~-mm diaphragm-~~ mm in diameter between the traps into the second measurement trap operating under ultrahigh vacuum ($\leq 10^{-7}$ mbar, estimated from vacuum system conductances), where the masses of ions can be measured or high-precision cleaning procedures applied. The RFQ is placed on a 30 kV high voltage platform, which defines the electric potential the ions leave the RFQ. The Penning traps are on a high voltage platform that is 54 V higher than the RFQ platform. This way it is enough to use only negative DC power supplies for trap electrodes. No pulsed drift tubes [40,41] to change ions' electric potential are used in the whole setup. The MCP detector is located outside the strong magnetic field at the ground potential and thus the extracted ions will hit the detector with $30z$ keV of energy. The magnetic field in the traps and in the region of the detector is about 7 T and 45 mT, respectively.

The extraction part ~~after the traps~~ of the JYFLTRAP was modified to better serve the PI-ICR technique (see Fig. 3). The inner diameter of the last two extraction electrodes and the ground electrode was increased from 32 mm up to 52 mm. A position-sensitive MCP ion detector with a delay-line anode (DLD40) from RoentDek GmbH [42] is placed on a feedthrough at a distance of about 923 mm from the center of the second trap. The detector is fully movable in the plane perpendicular to the beam and can also be fully retracted from the beam enabling the beam delivery to experiments further downstream. An einzel lens for transporting the ion beam towards post-trap decay spectroscopy setups is placed on the same feedthrough.

The voltages applied to the electrodes in the measurement trap and the extraction electrodes used for PI-ICR technique are shown in Table 1. The procedure of the optimization of voltages on the correction trap electrodes is described in Section 3.2. The first trap has the same trap potential $U_0 = 100$ V as the second trap.

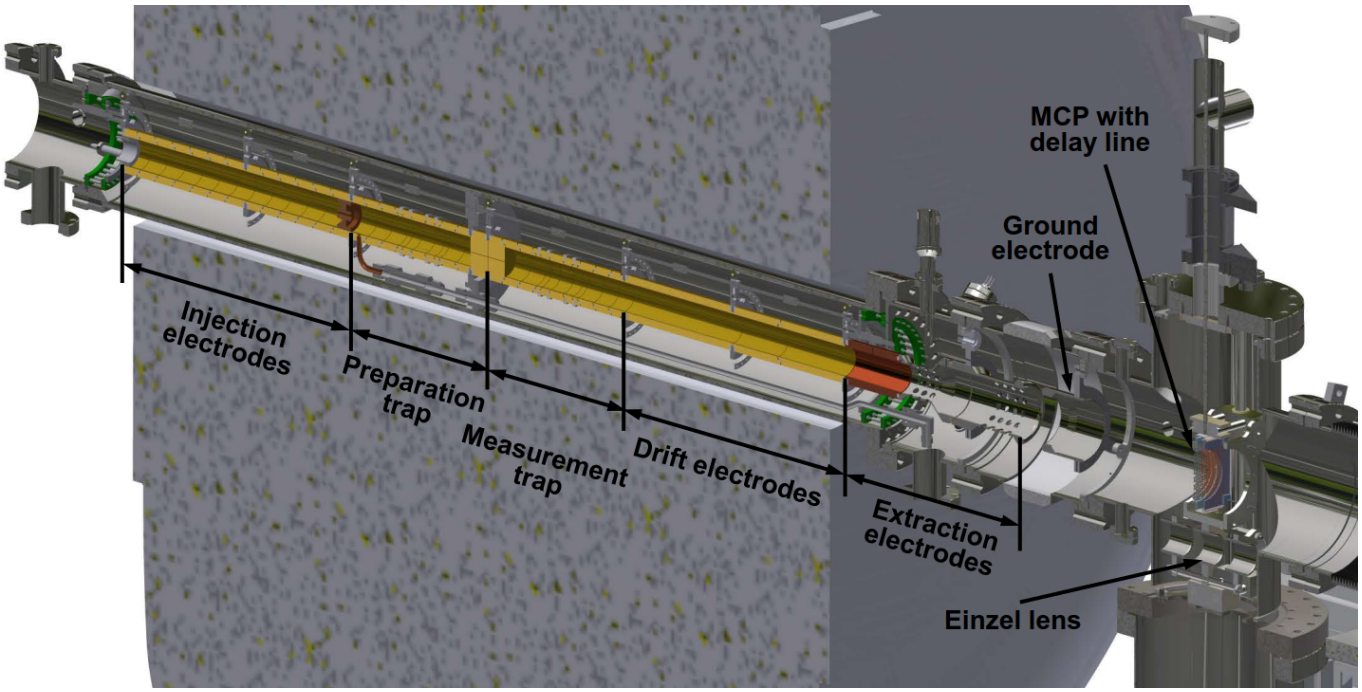

Fig. 3. The electrodes inside the superconducting magnet forming the Penning traps and extraction part of the setup outside the magnet (a half-cut view). The ground electrode is located inside an insulator, which separates the high voltage and ground sides. An MCP detector with a delay-line anode is located on the axis of the traps outside the magnet, where the magnetic field is weak; its position can be changed in the radial plane.

Table 1. Voltages on the electrodes of the measurement trap and extraction electrodes relative to the trap high voltage level, used for the PI-ICR technique. The "trapping" voltages are used to store ions in the trap and "Inj. / Extr." voltages are for injecting or extracting the ions into/from the trap.

Electrode	Trapping (V)	Inj./Extr. (V)
Endcaps	-10	-130
Correction 2 Injection	-44	-130
Correction 1 Injection	-94.66	-130
Ring	-110	-110
Correction 1 Extraction	-94.66	-131
Correction 2 Extraction	-44	-131
Endcaps	-10	-131
Drift1		-500
Drift2		-500
Drift3		-500
Extraction 1		-500
Extraction 2		-500
Extraction 3		-500

Fig. 4 shows trajectories of ions leaving the second trap with an initial magnetron radius $r_- = 1$ mm simulated using the SIMION program [43]. Potentials on the drift and extraction electrodes were set to -500 V (all voltages except the ground electrode are relative to the trap high voltage platform level). Ions follow the diverging magnetic field lines in the region of constant electric potential. Then, near the ground electrode they have an intermediate focus point due to the transition from high voltage to the ground potential, thereafter the ion beam (that now has $30z$ keV of energy) diverges again. The projection of ions linearly magnifies the image on the detector. The magnification of the image on the detector depends on the ratio of the magnetic field in the trap to the magnetic field in the detector region, the drift potential (potentials on the drift and extraction electrodes) and the distance of the detector from the ground electrode. In our case the magnification factor is about 10.2. Measured projections of ion radial motions are shown in Fig. 5.

3.2 Quadrupole elecrostatic potential optimizations with simulations and PI-ICR technique

Imperfections of the electrostatic field, *i.e.*, deviation of the trapping potential from the quadratic form (Eq. 2), ~~results~~ result in amplitude-dependent eigenfrequency shifts in a Penning trap. The purely quadratic potential of Eq. (2) can be expanded by adding higher order multipole terms. With the addition of octupolar and dodecapolar terms, characterized by the coefficients C_4 and C_6, respectively, the trapping potential is expressed as [44]:

$$V(z,\rho) = \frac{U_0}{2d^2}(z^2 - \frac{\rho^2}{2}) + C_4\frac{U_0}{2d^4}(z^4 - 3z^2\rho^2 + \frac{3}{8}\rho^4) + \\ + C_6\frac{U_0}{2d^6}(z^6 - \frac{15}{2}z^4\rho^2 + \frac{45}{8}z^2\rho^4 + \frac{5}{16}\rho^6). \quad (10)$$

The geometry of the JYFLTRAP Penning trap electrodes was simulated in COMSOL [45]. The contribution

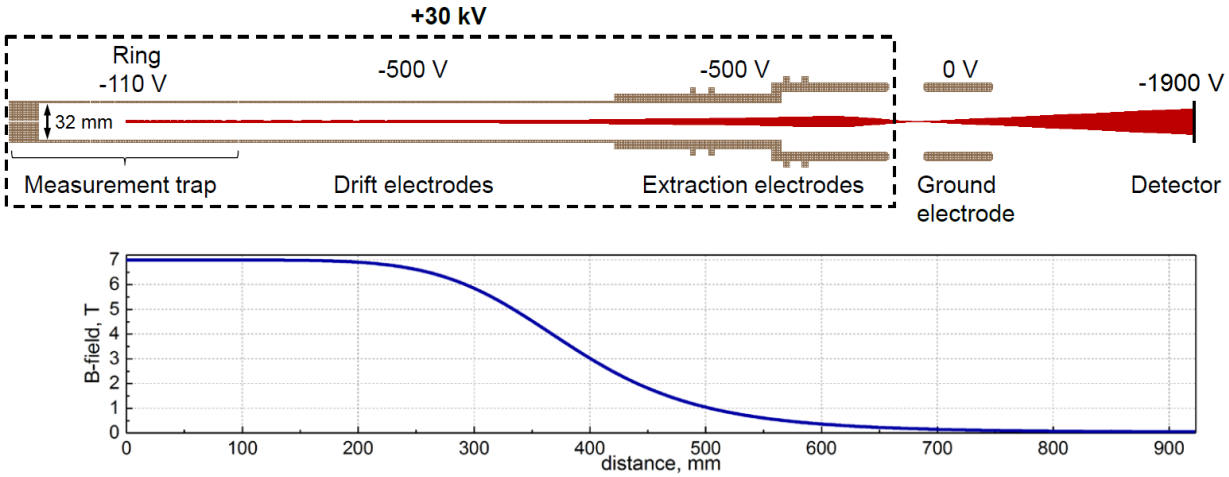

Fig. 4. (*Top*) Trajectory of ions (shown in red) leaving the second trap with an initial magnetron radius $r_- = 1$ mm simulated using Simion. (*Bottom*) Axial component of the magnetic field on the axis of the setup.

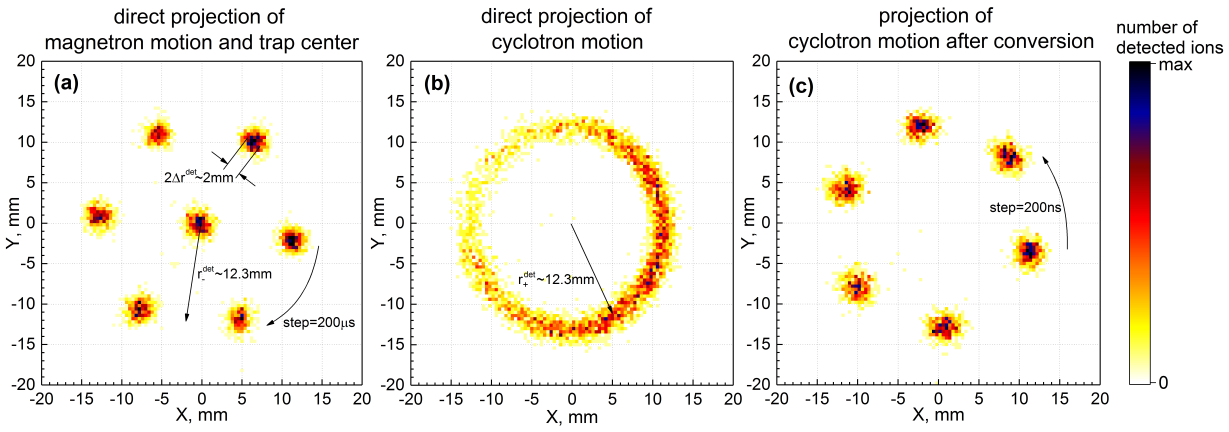

Fig. 5. Projections of ion radial motions with the short accumulation times (a few ms) on the detector, measured for $^{133}Cs^+$ ions. (*a*): Projection of 6 phases of the magnetron motion and trap center. (*b*): Direct projection of the cyclotron motion with a certain phase. (*c*): Projection of 6 phases of the cyclotron motion after the full conversion into the magnetron motion.

of each electrode to the electric field distribution in the radial plane along the $z = 0$ line was determined by setting 1 V on the electrode while keeping the others at zero. The superposition of such contributions multiplied by the voltage on each electrode forms the final trap potential. Firstly, the voltage between the endcap and the ring electrodes was fixed to 100 V. Then, the voltages on the trap electrodes Correction 1 and Correction 2 were tuned to minimize the coefficients C_4 and C_6 of Eq. (10). The final values for the voltages on the correction electrodes are shown in Table 1.

The harmonicity of the trap can be checked and fine-tuned further with the PI-ICR technique. If the trapping potential is purely quadratic and no higher order components are present, the eigenfrequencies of the ions do not depend on motional amplitudes. This can be observed by exciting the ions to different amplitudes and observing the extracted motional phase. If the frequency has no amplitude dependence, *i.e.*, the motion is harmonic, the extracted ions should form a straight line on the detector. The longer the accumulation time, the higher the sensitivity to the imperfections of the electric field. The magnetron motion is the most convenient to use because the phase of the fast cyclotron motion will get smeared due to the collisions of ions with the molecules of residual gas in the measurement trap. The shift of the magnetron frequency in the presence of the octupolar and dodecapolar components in the trapping potential is [44]:

$$\Delta\nu_- = \frac{\nu_+\nu_-}{\nu_+ - \nu_-}\left[\left(\frac{-3C_4}{2d^2} + \frac{45C_6}{4d^4}(r_-^2 - z^2)\right)r_-^2 + \right.$$
$$\left. + \frac{15C_6}{8d^4}r_-^4 + C(C_4, C_6)\right], \quad (11)$$

where r_-, r_+ and z are the amplitude of magnetron motion, cyclotron motion and axial motion, respectively; $C(C_4, C_6)$ is a constant, which does not depend on r_-.

Fig. 6 shows the phase spots for different magnetron radii after a phase accumulation time of 1 s. A measurement with $r = 1.03$ mm was taken as the reference. The fits for this dependence (Fig. 6b) with the polynomials $a + br_-^2$ and $a + br_-^2 + dr_-^4$ showed that coefficients b and

d are compatible with zero. The reduced χ^2/n for the fit with the constant function is 1.3 and even smaller than for polynomials. The estimated upper limit for the octupolar coefficient is $|C_4| < 7 \cdot 10^{-4}$.

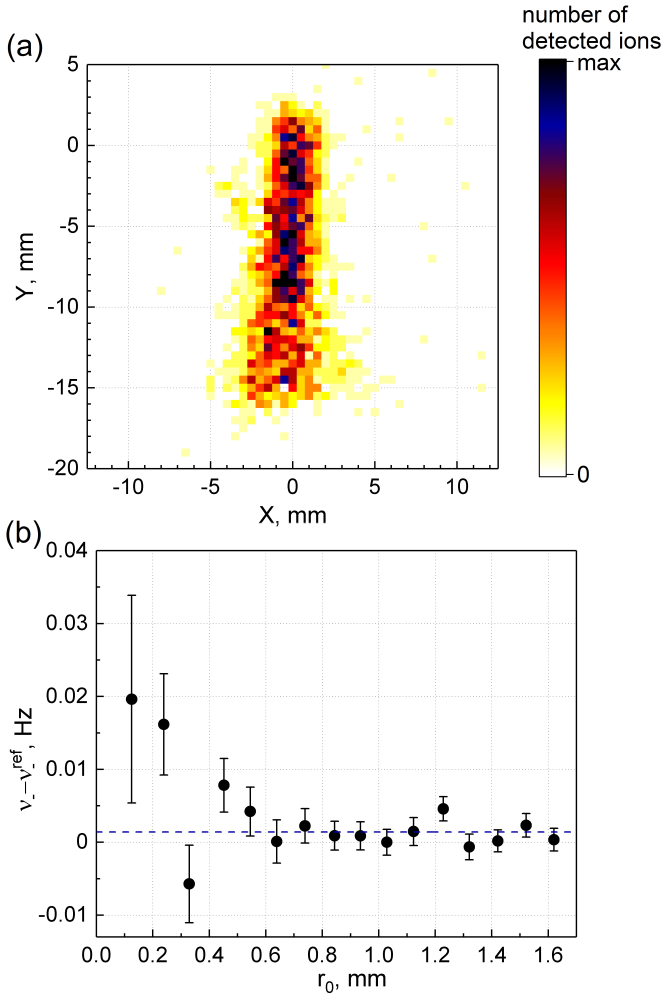

Fig. 6. (a): Image of the magnetron phases of $^{133}Cs^+$ ions on the detector for different magnetron radii after phase accumulation time of 1 s. The measurement was done after the optimization of the correction electrode voltages. The amplitude of a 1-ms magnetron excitation pulse was scanned bunch-by-bunch from 0.02 V to 0.82 V during the data collection. (b): Obtained shift of the magnetron frequency with respect to the reference magnetron frequency ($\sim$ 1700 Hz) at the magnetron radius $r_0 = 1.03$ mm as a function of the magnetron radius. The dashed line represents the average value.

3.3 Mass measurements of stable ions with the PI-ICR technique

The mass difference between the isotopes ^{87}Rb and ^{85}Rb was determined by measuring the cyclotron frequency ratio $R = \nu_c(^{85}Rb^+)/\nu_c(^{87}Rb^+)$ with the PI-ICR scheme described in Section 2.2.2. The $^{85}Rb^+$ and $^{87}Rb^+$ ions were produced with the surface-ionization ion source located in front of the RFQ cooler. The continuous ion beam from the source was cooled and bunched with the RFQ and transferred into the preparation trap, where the ions were cooled, centered and mass-separated. The cyclotron frequency measurements were performed in the measurement trap with a 200-ms phase accumulation time and alternately for $^{85}Rb^+$ and $^{87}Rb^+$ by changing the isotope every 5 minutes. The length of the measurement cycle was about 485 ms for pattern 1 and 2, that were applied alternately. During a 5-min long ~~single~~ measurement of the cyclotron frequency, about 600 ions were collected for both the magnetron and the cyclotron phase images. A two-dimensional scan of the start time of the dipolar excitation pulse at frequency ν_+ over a magnetron period (≈ 600 μs) and the start time of the extraction pulse over a cyclotron period (≈ 0.8 μs) was carried out (see pulse scheme in Fig. 2) to eliminate the shifts due to possible residual magnetron motion left after the magnetron amplitude reducing dipolar excitation and residual cyclotron motion after the conversion pulse. To reduce the errors due to possible distortions of ion-motion projection onto the detector the positions of the two phase images were chosen in such a way that the angles $|\alpha_c| \leq 2.5°$ during the measurements.

Count-rate analysis [46] for the determined cyclotron frequencies was performed to study ion-ion interactions. The data were divided into five groups according to the detected ions in bunches. No dependence of the frequency ratio on the number of detected ions were observed and only the data with up to 5 ions/bunch were taken into account. For a single frequency ratio measurement, the cyclotron frequency of $^{85}Rb^+$ was linearly interpolated to the measurement time of $^{87}Rb^+$ between the two $^{85}Rb^+$ measurements. The nonlinear drift of the magnetic field between two neighboring frequency measurements was negligible compared with the statistical errors. A typical distribution of $^{85}Rb^+$ ions on the detector for a single cyclotron frequency measurement is shown in Fig. 7.

During two ~~separate~~ measurement days 58 cyclotron frequency ratios $R = \nu_c(^{85}Rb^+)/\nu_c(^{87}Rb^+)$ were measured (Fig. 8~~.~~). The weighted mean ratio $\overline{R} = 1.023523278677(654)_{sta}$ results in a Q-value $(m(^{87}Rb^+) - m(^{85}Rb^+))c^2 = 1860557.540(52)$ keV. The Birge ratio [47] was 0.91, which indicates that the statistical errors for the ratios R are slightly overestimated. The larger internal uncertainty was used for the weighted mean of the frequency ratios. The received cyclotron frequency ratio $\overline{R}$ is in a perfect agreement with the Atomic Mass Evaluation 2016 (AME2016) value $R_{AME} = 1.023523278693(96)$ [20]. The difference $(-2 \pm 66) \cdot 10^{-11}$ for the frequency ratio or 1(52) eV for the Q-value is comparable with zero.

The cyclotron frequency ratios were also analyzed using a different approach. The frequencies in time t were

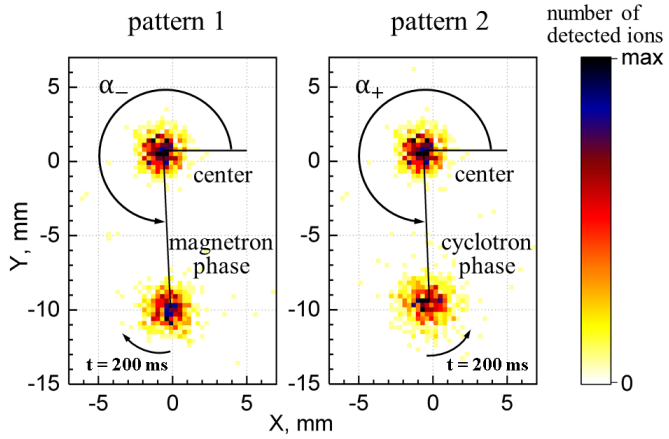

Fig. 7. The trap center and accumulated phase spots for $^{85}Rb^+$ ions on the position-sensitive ion detector. The magnetron-motion phase was accumulated using pattern 1 and the cyclotron-motion phase with pattern 2 of the excitation-pulse scheme.

simultaneously fitted with fifth-order polynomials

$$\nu_c(^{87}\mathrm{Rb}^+) = \sum_{i=0}^{5} a_i t^i \quad \text{and}$$

$$\nu_c(^{85}\mathrm{Rb}^+) = R_{day} \times \sum_{i=0}^{5} a_i t^i, \qquad (12)$$

where R_{day} is the cyclotron frequency ratio and the coefficients a_i are the same for both polynomials (see Fig. 9). The weighted mean ratio for two days $\overline{R} = 1.023523278629(662)_{stat}$ is similar to the frequency ratio received in the interpolation method and differs from it by $(-5 \pm 90) \cdot 10^{-11}$.

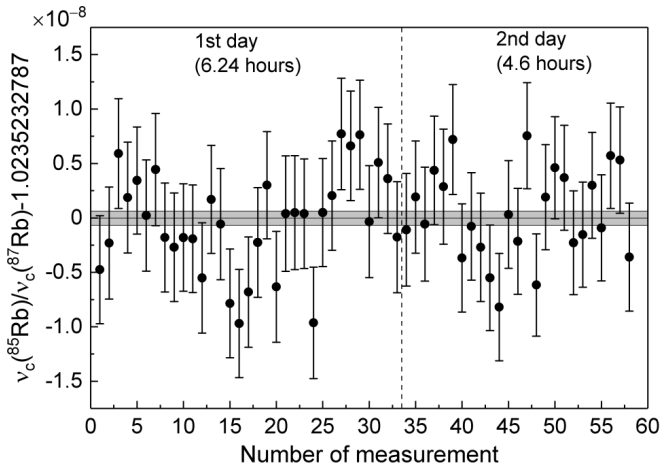

Fig. 8. Cyclotron frequency ratios of the $^{85}Rb^+$ and $^{87}Rb^+$ ions measured at JYFLTRAP in this work with the PI-ICR technique using 200 ms of accumulation time. The black line and shaded band are the weighted mean ratio $\overline{R}$ and its uncertainty.

The main systematic uncertainties were estimated. The maximum of possible cyclotron frequency ratio shift due to electrostatic imperfections of the trapping potential, that lead to the cyclotron frequency shifts [44]

$$\Delta\nu_c = -C_4 \frac{3}{2d^2} \frac{\nu_+\nu_-}{\nu_+ - \nu_-}(r_+^2 - r_-^2), \qquad (13)$$

was estimated as $|\Delta R_{\mathrm{elec}}| \leq 10^{-10}$, by using the upper limit for the coefficient C_4 (Sec. 3.2). For the cyclotron frequency ratio of mass doublet the ratio shift $|\Delta R_{\mathrm{elec}}|$ would be significantly less, because the frequencies (and their shifts) are very similar in this case. The shift due to distortions of ion-motion projection onto the detector [15] $|\Delta R_{\mathrm{orb}}|$ was also below 10^{-10}, since the angles α_c were close to zero. There is an uncertainty related to the drift of the image of the trap center on the detector, since we determined its position only before and after several hours of measurements of the magnetron-motion and cyclotron-motion phases. With the typical drift velocity of the center's coordinate of the image on the detector, which does not exceed 25 μm/h at JYFLTRAP, the frequency ratio shift $|\Delta R_{cent}|$ is less than 10^{-10}. Comprehensive systematic studies are under way and results of these will be published in the near future.

3.4 Online demonstration of phase-dependent cleaning method

The phase-dependent cleaning method (described in Sec. 2.3) was tested with radioactive $^{127}In^+$ ions produced in fission reaction of U with a 30-MeV proton beam. The ions of the ground and the first isomeric state, $^{127}In^+$ ($T_{1/2}$ = 1.09(1) s [48]) and $^{127m}In^+$ ($T_{1/2}$ = 3.67(4) s, E = 408.9(3) keV [48]), have a cyclotron frequency difference of about 3 Hz. This is large enough a difference that the states can also be isolated with the Ramsey cleaning method [28]. Here, the Ramsey cleaning method was used as an independent means to identify the states. The scan of dipolar excitation frequency (see Fig. 10) shows separated peaks for $^{127}In^+$ and $^{127m}In^+$ in the region of their modified cyclotron frequencies. One of the two states can be chosen by setting the appropriate frequency of the dipolar cleaning excitation. Thus, we can keep either the ground or the isomeric state using the Ramsey cleaning technique, or study both states when no Ramsey cleaning is applied.

Firstly, both the ground and the first isomeric states of $^{127}In^+$ were injected into the measurement trap. A 1-ms long dipolar excitation pulse at ν_+ frequency was applied and the ions were left for $\approx$160 ms to obtain a phase difference of about π. Finally, a 2-ms long quadrupolar conversion pulse at ν_c frequency was applied to convert the cyclotron motion to magnetron motion. The two states are clearly separated on the position-sensitive ion detector (see Fig. 11a). When using Ramsey cleaning to remove the ground state ions, only the right spot remains on the detector; and when the isomer is removed, the left spot remains. Thus, as it was expected from Fig. 10, the spot

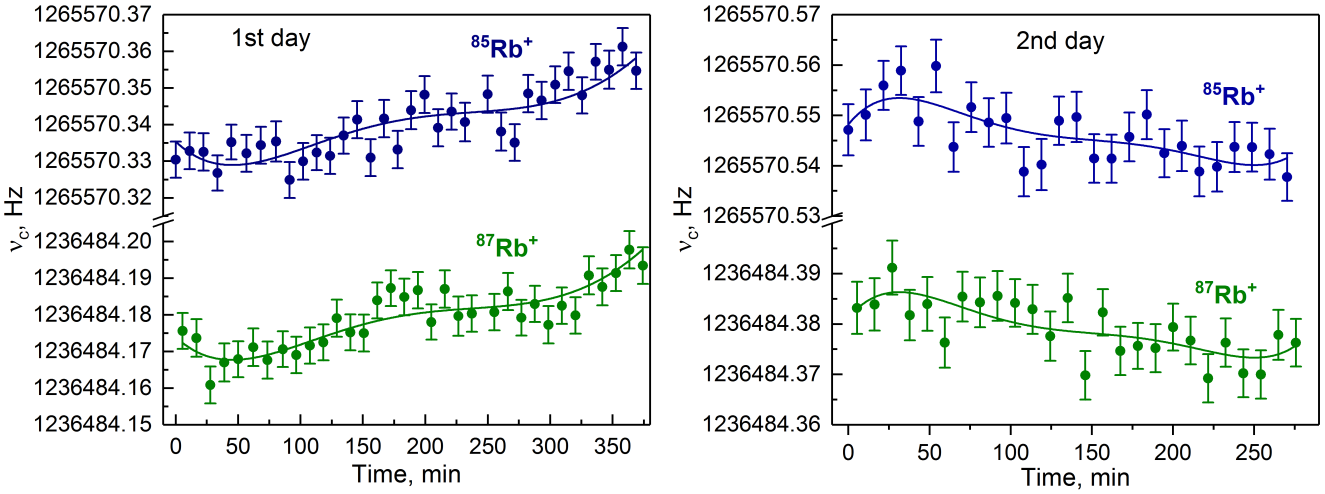

Fig. 9. The cyclotron frequency ratios R_{day} for each day were obtained by fitting fifth-order polynomials simultaneously to the ^{85}Rb$^+$ and ^{87}Rb$^+$ frequency points (see text for details). The reduced χ^2/n was 0.81 and 0.77 for the first and the second day, respectively. There were 5 days between the 1st and the 2nd day of the measurements.

with the higher number of detected ions corresponds to the more populated ground state.

After the two states were separated to have opposite motional phases, an additional dipolar excitation pulse at the magnetron frequency ν_- was applied to move the ground state ions of ^{127}In$^+$ towards the trap center (Fig. 11b) Since the amplitude and the phase of the dipolar pulse was chosen so that the ground state ions are centered while the isomeric state ions, having opposite motional phase with respect to the the dipolar field, move further away. When contaminants and the ion-of-interest have a phase difference of π, the contaminants can be driven to orbit with twice the radius. If the contaminants are driven to large enough orbit, they will be lost upon extraction. In the case shown in Fig. 11d, the ions of ^{127m}In$^+$ are placed about 23 mm away from the center of the detector, a distance that is larger than the radius of the detector. When the detector is removed and the einzel lens with a 16 mm inner radius is put in its place, the contaminants will be lost.

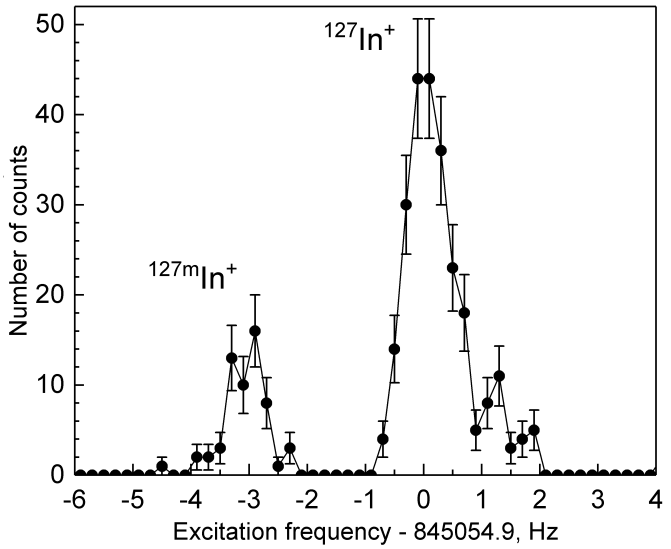

Fig. 10. Number of detected ions as a function of applied frequency of dipolar excitation using a timing pattern 5-70-5 ms (On-Off-On) in the Ramsey cleaning method.

4 Conclusion

The Phase-Imaging Ion-Cyclotron-Resonance technique has been successfully commissioned and implemented at JYFLTRAP. The performance was tested with the stable ions ^{133}Cs$^+$, ^{85}Rb$^+$ and ^{87}Rb$^+$ using a surface ionization ion source. The voltages on the Penning trap electrodes were optimized to reduce higher order terms in the trapping potential and minimize related systematic errors. The accuracy of the PI-ICR technique was tested with ^{85}Rb$^+$ and ^{87}Rb$^+$ ions. The measured cyclotron frequency ratio is in an agreement with the AME2016 value [20]. Thus, even at such a high level of accuracy of around $6.4 \cdot 10^{-10}$, we do not observe systematic shifts in the PI-ICR mass measurement, even for ions which are not from the same mass doublet.

A new phase-dependent cleaning method was demonstrated with short-lived ^{127}In$^+$ ions. The ground and first isomeric state of ^{127}In were separated by accumulating the phase difference of about π of cyclotron motion in the trap. An additional excitation pulse at the magnetron frequency (with proper phase and amplitude) centered the ions of one state while the ions of the other state gained even bigger radius. If this is chosen to be bigger than the inner radius of the einzel lens, the contaminants will be lost after extraction from the trap. The installation of adjustable slits in front of the position sensitive ion detector will enable cleaning with the accumulated phase difference smaller than π. This increases the resolving power

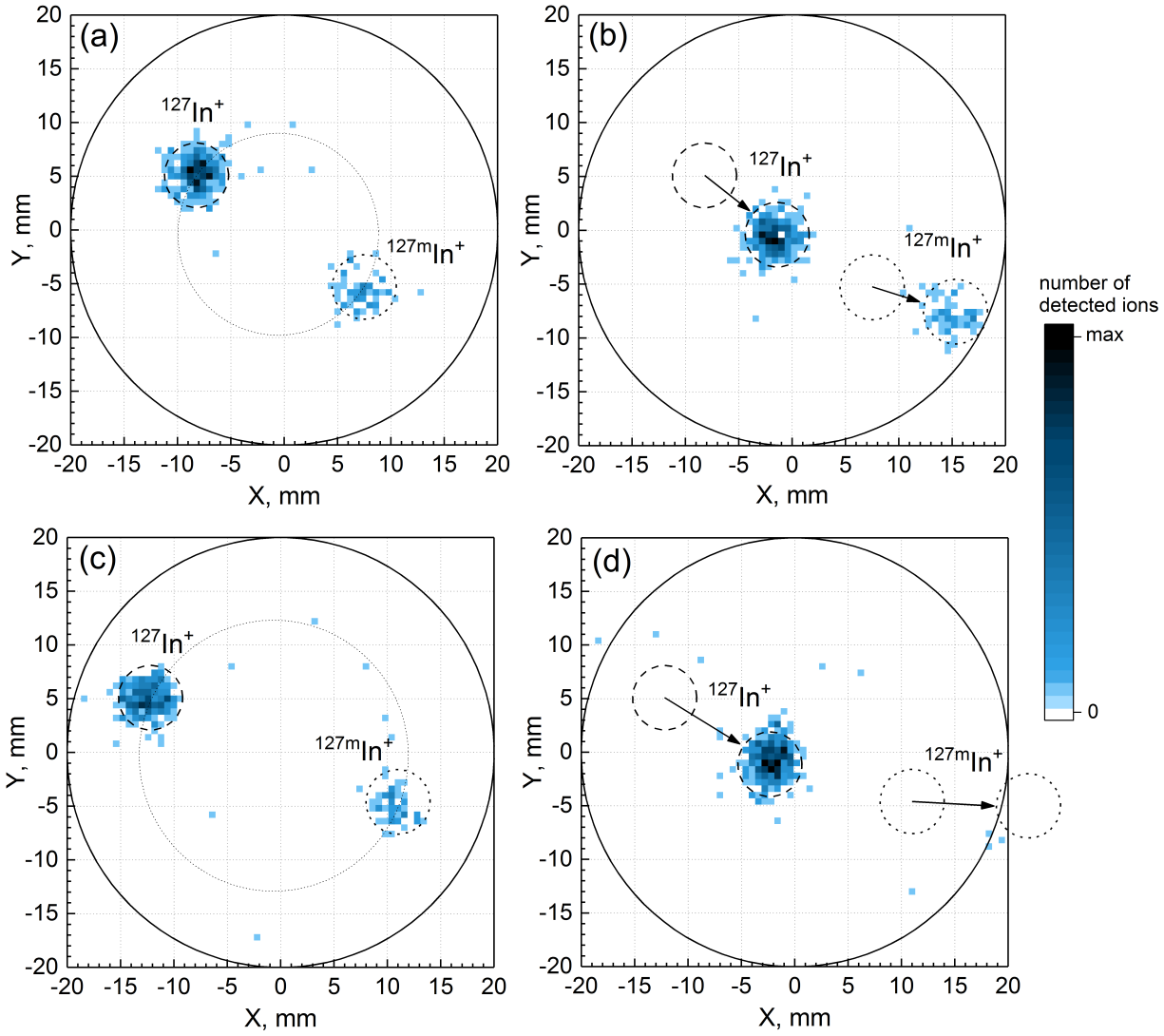

Fig. 11. Image of ion distribution for the ground and first isomeric states of ^{127}In$^+$ on the position-sensitive ion detector. The big circle with a ∼20 mm radius depicts (roughly) the outer edge of the position sensitive ion detector. (*a*):The ions were extracted from the trap after first accumulating the phase of the cyclotron motion for 160 ms and conversion to magnetron motion. The amplitude of the 1-ms pulse for the ν_+-excitation was $A_+ = 0.9$ V and $A_c = 3$ V for the 2-ms long conversion pulse. (*b*): As *(a)* with additional dipolar excitation pulse at the magnetron frequency (amplitude $A_- = 0.85$ V, applied for one magnetron period ($\sim 600\,\mu$s)) before the extraction. ^{127}In$^+$ ions move to the center while ^{127m}In$^+$ ions moves further out. (*c*) and (*d*): the same images as in (*a*) and (*b*), but with the higher amplitudes for ν_+- and ν_--excitations ($A_+ = 1.2$ V for 1 ms, $A_- = 1.13$ V for one magnetron period). Since the two states do not exactly have 1π phase difference, the spots in (b) and (d) do not move exactly to the same direction.

or, alternatively, decreases the time needed for the cleaning process.

Acknowledgements

This work has been supported by the Academy of Finland under the Finnish Centre of Excellence Programme 2012-2017 (Nuclear and Accelerator Based Physics Research at JYFL) and by the project "State-of-the-art ion beam developments for JYFL-ACCLAB", decision No. 273526. A.K. acknowledges the support from the Academy of Finland under grant No. 275389 and D.N. and L.C. under grants No. 284516 and 312544. T.E. acknowledges the support from the Academy of Finland under grant No. 295207 and A.R. under grant No. 306980.

References

1. K. Blaum, J. Dilling, W. Nörtershäuser, Precision atomic physics techniques for nuclear physics with radioactive beams, Physica Scripta 2013 (T152) (2013) 014017. doi:10.1088/0031-8949/2013/T152/014017.
2. T. Eronen, A. Kankainen, J. Äystö, Ion traps in nuclear physics-recent results and achievements, Progress in Par-

ticle and Nuclear Physics 91 (2016) 259 – 293. doi:10.1016/j.ppnp.2016.08.001.
3. T. Eronen, J. C. Hardy, High-precision Q_{EC} -value measurements for superallowed decays, The European Physical Journal A 48 (4) (2012) 48. doi:10.1140/epja/i2012-12048-y.
4. S. Eliseev, T. Eronen, Y. N. Novikov, Penning-trap mass spectrometry for neutrino physics, Int. J. Mass Spectrom. 349–350 (2013) 102–106. doi:10.1016/j.ijms.2013.03.010.
5. G. Gräff, H. Kalinowsky, J. Traut, A direct determination of the proton electron mass ratio, Z. Phys. A 297 (1) (1980) 35–39. doi:10.1007/BF01414243.
6. M. König, G. Bollen, H. J. Kluge, T. Otto, J. Szerypo, Quadrupole excitation of stored ion motion at the true cyclotron frequency, Int. J. Mass Spectrom. Ion Processes 142 (1-2) (1995) 95 – 116. doi:10.1016/0168-1176(95)04146-C.
7. S. George, et al., Ramsey method of separated oscillatory fields for high-precision penning trap mass spectrometry, Phys. Rev. Lett. 98 (2007) 162501. doi:10.1103/PhysRevLett.98.162501.
8. S. George, K. Blaum, F. Herfurth, A. Herlert, M. Kretzschmar, S. Nagy, S. Schwarz, L. Schweikhard, C. Yazidjian, The Ramsey method in high-precision mass spectrometry with penning traps: Experimental results, Int. J. Mass Spectrom. 264 (23) (2007) 110 – 121. doi:10.1016/j.ijms.2007.04.003.
9. M. Kretzschmar, The Ramsey method in high-precision mass spectrometry with penning traps: Theoretical foundations, International Journal of Mass Spectrometry 264 (23) (2007) 122 – 145. doi:10.1016/j.ijms.2007.04.002.
10. M. Goncharov, K. Blaum, M. Block, C. Droese, S. Eliseev, F. Herfurth, E. Minaya Ramirez, Y. N. Novikov, L. Schweikhard, K. Zuber, Probing the nuclides ^{102}Pd, ^{106}Cd, and ^{144}Sm for resonant neutrinoless double-electron capture, Phys. Rev. C 84 (2011) 028501. doi:10.1103/PhysRevC.84.028501.
11. D. A. Nesterenko, et al., High-precision mass measurements for the isobaric multiplet mass equation at A = 52, Journal of Physics G: Nuclear and Particle Physics 44 (6) (2017) 065103. doi:doi.org/10.1088/1361-6471/aa67ae.
12. E. M. Ramirez, et al., Direct mapping of nuclear shell effects in the heaviest elements, Science 337 (6099) (2012) 1207–1210. doi:10.1126/science.1225636.
13. J. Hakala, et al., Precision mass measurements of neutron-rich Y, Nb, Mo, Tc, Ru, Rh, and Pd isotopes, The European Physical Journal A 47 (10) (2011) 129. doi:10.1140/epja/i2011-11129-9.
14. S. Eliseev, K. Blaum, M. Block, C. Droese, M. Goncharov, E. Minaya Ramirez, D. A. Nesterenko, Y. N. Novikov, L. Schweikhard, Phase-imaging ion-cyclotron-resonance measurements for short-lived nuclides, Phys. Rev. Lett. 110 (2013) 082501. doi:10.1103/PhysRevLett.110.082501.
15. S. Eliseev, et al., A phase-imaging technique for cyclotron-frequency measurements, Applied Physics B 114 (1) (2014) 107–128. doi:10.1007/s00340-013-5621-0.
16. D. A. Nesterenko, et al., Direct determination of the atomic mass difference of ^{187}Re and ^{187}Os for neutrino physics and cosmochronology, Phys. Rev. C 90 (2014) 042501. doi:10.1103/PhysRevC.90.042501.
17. S. Eliseev, et al., Direct measurement of the mass difference of ^{163}Ho and ^{163}Dy solves the Q-value puzzle for the neutrino mass determination, Phys. Rev. Lett. 115 (2015) 062501. doi:10.1103/PhysRevLett.115.062501.
18. F. Köhler, et al., Isotope dependence of the zeeman effect in lithium-like calcium, Nature Communications 7 (2016) 10246. doi:10.1038/ncomms10246.
19. T. Eronen, et al., JYFLTRAP: a Penning trap for precision mass spectroscopy and isobaric purification, Eur. Phys. J. A 48 (4) (2012) 46. doi:10.1140/epja/i2012-12046-1.
20. M. Wang, G. Audi, F. Kondev, W. Huang, S. Naimi, X. Xu, The AME2016 atomic mass evaluation (ii). tables, graphs and references, Chinese Physics C 41 (3) (2017) 030003.
21. G. Bollen, H.-J. Kluge, M. König, T. Otto, G. Savard, H. Stolzenberg, R. B. Moore, G. Rouleau, G. Audi, I. Collaboration, Resolution of nuclear ground and isomeric states by a penning trap mass spectrometer, Phys. Rev. C 46 (1992) R2140–R2143. doi:10.1103/PhysRevC.46.R2140.
22. G. Savard, S. Becker, G. Bollen, H. J. Kluge, R. B. Moore, T. Otto, L. Schweikhard, H. Stolzenberg, U. Wiess, A new cooling technique for heavy ions in a penning trap, Phys. Lett. A 158 (5) (1991) 247 – 252. doi:10.1016/0375-9601(91)91008-2.
23. M. Rosenbusch, K. Blaum, C. Borgmann, S. Kreim, M. Kretzschmar, D. Lunney, L. Schweikhard, F. Wienholtz, R. Wolf, Buffer-gas-free mass-selective ion centering in penning traps by simultaneous dipolar excitation of magnetron motion and quadrupolar excitation for interconversion between magnetron and cyclotron motion, International Journal of Mass Spectrometry 325-327 (2012) 51 – 57. doi:10.1016/j.ijms.2012.06.008.
24. R. Wolf, et al., ISOLTRAP's multi-reflection time-of-flight mass separator/spectrometer, Int. J. Mass Spectrom. 349-350 (2013) 123–133. doi:10.1016/j.ijms.2013.03.020. URL http://dx.doi.org/10.1016/j.ijms.2013.03.020
25. R. Ringle, G. Bollen, P. Schury, S. Schwarz, T. Sun, Octupolar excitation of ion motion in a penning trapa study performed at LEBIT, International Journal of Mass Spectrometry 262 (1) (2007) 33 – 44. doi:10.1016/j.ijms.2006.10.009.
26. S. Eliseev, M. Block, A. Chaudhuri, F. Herfurth, H.-J. Kluge, A. Martin, C. Rauth, G. Vorobjev, Octupolar excitation of ions stored in a penning trap mass spectrometera study performed at shiptrap, International Journal of Mass Spectrometry 262 (1) (2007) 45 – 50. doi:https://doi.org/10.1016/j.ijms.2006.10.003.
27. A. T. Gallant, et al., Highly charged ions in penning traps: A new tool for resolving low-lying isomeric states, Phys. Rev. C 85 (2012) 044311. doi:10.1103/PhysRevC.85.044311.
28. T. Eronen, V.-V. Elomaa, U. Hager, J. Hakala, A. Jokinen, A. Kankainen, S. Rahaman, J. Rissanen, C. Weber, J. Äystö, Preparing isomerically pure beams of short-lived nuclei at JYFLTRAP, Nucl. Instrum. Meth. Phys. Res. B 266 (1920) (2008) 4527 – 4531, Proceedings of the XVth International Conference on Electromagnetic Isotope Separators and Techniques Related to their Applications. doi:10.1016/j.nimb.2008.05.076.
29. L. S. Brown, G. Gabrielse, Geonium theory: Physics of a single electron or ion in a penning trap, Rev. Mod. Phys. 58 (1986) 233–311. doi:10.1103/RevModPhys.58.233.

30. G. Gabrielse, L. Haarsma, S. Rolston, Open-endcap Penning traps for high precision experiments, Int. J. Mass Spectrom. Ion Process. 88 (2-3) (1989) 319–332. URL http://www.sciencedirect.com/science/article/pii/016811768985027X
31. G. Gabrielse, The true cyclotron frequency for particles and ions in a penning trap, International Journal of Mass Spectrometry 279 (2) (2009) 107 – 112. doi:doi.org/10.1016/j.ijms.2008.10.015.
32. M. Kretzschmar, On the phase dependence of the interconversion of the motional modes in a Penning trap by quadrupolar excitation, Int. J. Mass Spectrom. 309 (2012) 30 – 38. doi:10.1016/j.ijms.2011.08.022. URL http://www.sciencedirect.com/science/article/pii/S1387380611003630
33. K. Blaum, High-accuracy mass spectrometry with stored ions, Physics Reports 425 (1) (2006) 1 – 78. doi:10.1016/j.physrep.2005.10.011.
34. G. Bollen, S. Becker, H.-J. Kluge, M. Knig, R. Moore, T. Otto, H. Raimbault-Hartmann, G. Savard, L. Schweikhard, H. Stolzenberg, Isoltrap: a tandem penning trap system for accurate on-line mass determination of short-lived isotopes, Nuclear Instruments and Methods in Physics Research Section A: Accelerators, Spectrometers, Detectors and Associated Equipment 368 (3) (1996) 675 – 697. doi:/10.1016/0168-9002(95)00561-7.
35. M. Block, et al., Towards direct mass measurements of nobelium at SHIPTRAP, The European Physical Journal D 45 (1) (2007) 39–45. doi:10.1140/epjd/e2007-00189-2.
36. P. Dupré, D. Lunney, High-resolution mass separation by phase splitting and fast centering of ion motion in a Penning trap, International Journal of Mass Spectrometry 379 (2015) 33 – 45. doi:10.1016/j.ijms.2014.12.007.
37. I. Moore, et al., Towards commissioning the new IGISOL-4 facility, Nucl. Instrum. Meth. Phys. Res. B 317 (2013) 208 – 213, XVIth International Conference on Electro-Magnetic Isotope Separators and Techniques Related to their Applications, December 27, 2012 at Matsue, Japan. doi:10.1016/j.nimb.2013.06.036.
38. P. Karvonen, I. Moore, T. Sonoda, T. Kessler, H. Penttilä, K. Peräjärvi, P. Ronkanen, J. Äystö, A sextupole ion beam guide to improve the efficiency and beam quality at IGISOL, Nucl. Instrum. Meth. Phys. Res. B 266 (21) (2008) 4794 – 4807. doi:10.1016/j.nimb.2008.07.022.
39. A. Nieminen, J. Huikari, A. Jokinen, J. Äystö, P. Campbell, E. Cochrane, Beam cooler for low-energy radioactive ions, Nucl. Instrum. Meth. Phys. Res. A 469 (2) (2001) 244 – 253. doi:10.1016/S0168-9002(00)00750-6.
40. F. Herfurth, et al., A linear radiofrequency ion trap for accumulation, bunching, and emittance improvement of radioactive ion beams, Nuclear Instruments and Methods in Physics Research Section A: Accelerators, Spectrometers, Detectors and Associated Equipment 469 (2) (2001) 254 – 275. doi:https://doi.org/10.1016/S0168-9002(01)00168-1.
41. T. Brunner, et al., TITAN's digital RFQ ion beam cooler and buncher, operation and performance, Nuclear Instruments and Methods in Physics Research Section A: Accelerators, Spectrometers, Detectors and Associated Equipment 676 (2012) 32 – 43. doi:doi.org/10.1016/j.nima.2012.02.004.
42. MCP delay line detector, RoentDek Handels GmbH. URL http://www.roentdek.de
43. SIMION, Scientific Instrument Services, Inc. (SIS). URL http://simion.com
44. J. Ketter, T. Eronen, M. Höcker, S. Streubel, K. Blaum, First-order perturbative calculation of the frequency-shifts caused by static cylindrically-symmetric electric and magnetic imperfections of a Penning trap, International Journal of Mass Spectrometry 358 (2014) 1 – 16. doi:10.1016/j.ijms.2013.10.005.
45. COMSOL, Inc. URL https://www.comsol.com
46. A. Kellerbauer, K. Blaum, G. Bollen, F. Herfurth, H.-J. Kluge, M. Kuckein, E. Sauvan, C. Scheidenberger, L. Schweikhard, From direct to absolute mass measurements: A study of the accuracy of isoltrap, The European Physical Journal D - Atomic, Molecular, Optical and Plasma Physics 22 (1) (2003) 53–64. doi:10.1140/epjd/e2002-00222-0. URL https://doi.org/10.1140/epjd/e2002-00222-0
47. R. T. Birge, The calculation of errors by the method of least squares, Phys. Rev. 40 (1932) 207–227. doi:10.1103/PhysRev.40.207.
48. G. Audi, F. Kondev, M. Wang, W. Huang, S. Naimi, The NUBASE2016 evaluation of nuclear properties, Chinese Physics C 41 (3) (2017) 030001.